Proceedings Paper:
Cooper, JD, Ikonić, Z, Cunningham, JE et al. (4 more authors) (2013) Surface acoustic wave modulation of quantum cascade lasers. In: Proceedings of the International Conference on Advanced Optoelectronics and Lasers, CAOL. 2013 International Conference on Advanced Optoelectronics and Lasers (CAOL), 9-13 September 2013, Sudak. IEEE , 22 - 24. ISBN 9781479900183

https://doi.org/10.1109/CAOL.2013.6657513

Surface acoustic wave modulation of quantum cascade lasers

J. D. Cooper, Z. Ikonić, J. E. Cunningham, P. Harrison, M. Salih, A. G. Davies and E. H. Linfield
School of Electronic & Electrical Engineering,
University of Leeds, LS2 9JT, U.K.

(Invited Paper)

***Abstract*—In this work, a description is given of a simulation technique employed to model the interaction between surface acoustic waves and ridge-waveguide quantum cascade lasers (QCLs). Firstly, a finite-difference time-domain (FDTD) scheme for modelling acoustic wave propagation in arbitrary semiconductor structures is outlined, and verified by comparison with experimental measurements of the frequency response of surface acoustic wave transmission between interdigitated transmitters and receivers on a bulk crystal. The model is developed further to represent the ridge-waveguide as a prominence above the surface and the active region of the laser is accounted for by a free-charge region buried within the structure. The modulation of this free charge, or carrier concentration by the propagating surface acoustic wave, is then used as an input to a rate equation model of a QCL to show how the gain will be affected. It is this control of the gain through the amplitude of the surface acoustic wave which will allow for modulation of the mid-infrared or terahertz output of the laser and hence its incorporation in many new applications.**

I. Introduction

QUANTUM cascade lasers are n-type unipolar semiconductor heterostructure lasers fabricated from many repeats of an active region unit cell that is itself comprised of several quantum wells. The electron energy levels and lifetimes within an active region are engineered to create a population inversion between two levels which when coupled with a resonant cavity or waveguide can lead to gain (amplification). GaAs-based devices give quantum wells that are one or two hundred meV deep, with a spacing between electron energy levels of a few tens of meV and hence transitions between these states are typically in the mid- or far-infrared (terahertz) regions of the spectrum. These wavelengths have already been shown to be useful for chemical and biological sensing[1]. It is then of interest to achieve precise and continuous dynamical tuning of the laser wavelength, certainly within the limits set by the active transition linewidth. One possibility for this is to employ distributed feedback (DFB) lasers, rather than the conventional end-mirror resonator lasers, where the distributed feedback is provided by gain and refractive index modulation caused by a surface acoustic wave (SAW). The latter are generated by applying alternating voltages to interdigitated metallic fingers deposited on a surface which then form a transducer, producing a mechanical wave through the piezoelectric effect. This wave in turn will modulate the electron density within the active region of the laser, and hence the gain and the refractive index, providing an optical feedback. The operating frequency is thus tuned by changing the SAW frequency, i.e. the DFB grating period. Modulation of the laser intensity is also possible via the acoustic wave modulation depth, i.e. its power.

The schematic structure of the SAW-modulated QCL is shown in Fig. 1, where the QCL is placed on top of the SAW substrate in between two interdigitated transducers (IDTs), which can either generate or detect a SAW. Physically, the reason for having a second IDT is to check that a working SAW device has been fabricated. This is shown in this schematic for completeness and need not be included within the simulation when modelling the SAW propagation through the QCL ridge. Since the carrier concentration within the QCL active region will be modulated by the electric field of the SAW, generated via the piezoelectric effect, a portion of the SAW energy must move up into the QCL from the substrate for any modulation to be seen. The purpose of the simulation of SAW propagation is to determine how much of the SAW energy moves from the substrate, where it is generated by the transmitting IDT (TxIDT), into the QCL and modulates the active region. Because the structure does not vary in the direction parallel to the SAW wavefront (x_2), it is assumed that there is no variation in this direction therefore making the problem two-dimensional and greatly reducing the computational expense of finding a solution.

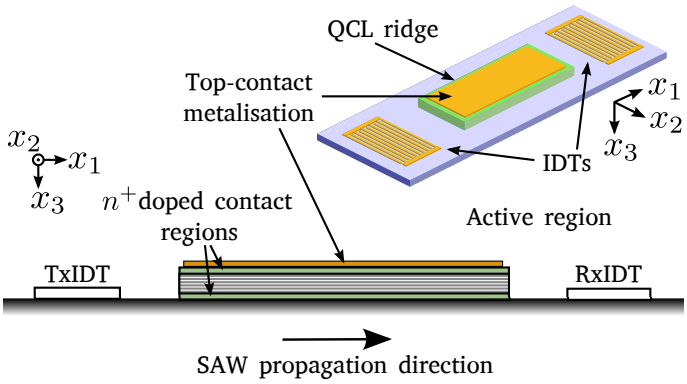

Fig. 1. Schematic diagram of the simulated device showing the transmitting and receiving IDTs (TxIDT/RxIDT) with the QCL ridge in the center. (Inset) Three-dimensional schematic of the device.

II. Theory

The equations of motion which govern acoustic wave propagation within a piezoelectric crystal are:

$$\rho \frac{\partial u_i}{\partial t} = \frac{\partial v_{ij}}{\partial x_j} \qquad \text{for } i, j = 1, 2, 3, \tag{1}$$

where ρ is the density of the material, u_i is displacement inside the material along the three orthogonal axes x_i and v is an auxiliary field whose time differential takes the form:

$$\begin{aligned} \frac{\partial v_i}{\partial t} &= \sigma_i = C_{ij}\epsilon_j + e_{ik}^T \frac{\partial \phi}{\partial x_k} \\ &\text{for } i, j = 1, \ldots, 6, \quad k = 1, 2, 3, \end{aligned} \tag{2}$$

where this auxiliary field is expressed in matrix notation rather than the tensor notation in equation (1), as described in [2]. σ is the stress, C is the elastic constant, ϵ is the strain, and ϕ is the potential. The strain, ϵ may be described in terms of displacement:

$$\begin{aligned} \epsilon_i &= \frac{\partial u_i}{\partial x_i} \qquad \text{for } i = 1, 2, 3, \\ \epsilon_4 &= \frac{1}{2}\left(\frac{\partial u_3}{\partial x_2} + \frac{\partial u_2}{\partial x_3}\right), \\ \epsilon_5 &= \frac{1}{2}\left(\frac{\partial u_3}{\partial x_1} + \frac{\partial u_1}{\partial x_3}\right), \\ \epsilon_6 &= \frac{1}{2}\left(\frac{\partial u_2}{\partial x_1} + \frac{\partial u_1}{\partial x_2}\right), \end{aligned} \tag{3}$$

to complete the set of equations. These are solved by discretising onto an interlaced mesh and using an FDTD forward-stepping algorithm, as described in [3], including perfectly-matched-layer boundary conditions to stop artificial reflections from the edges of the simulation domain. The potential within the piezoelectric crystal is assumed to be adiabatic and found by solving Poisson's equation for the strain-induced charge displacement, which is given by,

$$\rho = \frac{\partial}{\partial x_i} e_{ij}\epsilon_j \qquad \text{for } i = 1, 2, 3, \quad j = 1, \ldots, 6. \tag{4}$$

Because surface-bound propagation modes are to be simulated, i.e. SAWs, a surface boundary condition need to be imposed within the simulation domain. This requires that the components of stress which act across the surface boundary therefore vanish, defining the surface as perpendicular to the x_3 axis and at the point $x_3 = 0$,

$$\sigma_3 = \sigma_4 = \sigma_5 = 0 \qquad \text{at } x_3 = 0. \tag{5}$$

In order to excite the SAW, we mimic the potential profile generated by the IDT. Since the simulation domain is assumed invariant in the direction parallel to the wavefront, the potential is assumed to be invariant along the length of each IDT finger. The potential across each finger is also assumed to be constant as the movement of charge is very fast compared to the SAW propagation and is therefore considered adiabatic, as already stated. Mimicking the potential profile around the IDT therefore entails fixing the potential within the solution to Poisson's equation at the surface boundary condition imposed within the simulation domain, such that there are spatially alternating regions of positive and negative potential which oscillate from positive to negative in the time domain. This method of excitation is very general as it not only allows for any IDT structure (which is invariant along the wavefront) to be modelled by changing the positions and dimensions of the areas of fixed potential, but also the frequency and size of the applied field may be altered.

As the acoustic wave equations of motion will support all modes of acoustic wave propagation, the validity of using this method to excite SAWs must be checked. Initially, a simple visual check may be used to ensure that the majority of the acoustic wave energy exists near the surface, therefore ensuring a surface bound mode has been excited.

III. Comparison with experiment: SAW propagation in bulk

The simulated frequency response of a SAW device, consisting just of transmitting and receiving IDTs to generate and detect the SAW, similar to Fig. 1 but *without* the QCL ridge, was compared with experimental results. The results of these simulations are shown in the inset of Fig. 2 for the particular case of IDTs each with 40 finger-pairs. It can be seen that the form of the frequency response from the simulations matches that of the experimental measurements very well, though there is a consistent difference in the losses which may be accounted for by the lack of impedance matching between the co-axial lines and the transducers in the experiment. The full-width at half-maximum (FWHM) of the central peak, as evident in the inset, is a well-known characteristic of the response of IDTs and varies with the number of transducer finger pairs. With this in mind, several SAW devices were fabricated with varying numbers of finger pairs in the transmitting and receiving IDTs, and their measured frequency responses are compared to simulations of the same structures in the main part of Fig. 2. Again there is an excellent agreement between experiment and simulation which serves to validate the approach to simulating SAW propagation described here.

IV. Simulations of SAW propagation in a QCL

In order to simulate SAW propagation through a QCL ridge, the surface boundary condition must be altered to accommodate ridge structures. This may be done by using a similar surface boundary for vertical surfaces, such that the stresses across the vertical surface vanish, and then combining the two boundary conditions at the corner points by considering which elements of the stress tensor are zero. To simulate the screening effect of the charge within the QCL active region, as well as to determine the magnitude of the modulation of free carriers within the active region, a layer of free electrons is placed within the ridge structure along with a positive charge density to account for the ionised dopant atoms which donate the free charge. Since the quantum wells within the active region run parallel to the SAW propagation direction, and the in-plane mobility of electrons is much higher than in the direction through the quantum well structure, it is assumed that the free charge can only move in the direction parallel to the SAW propagation. It is also assumed that movement of the

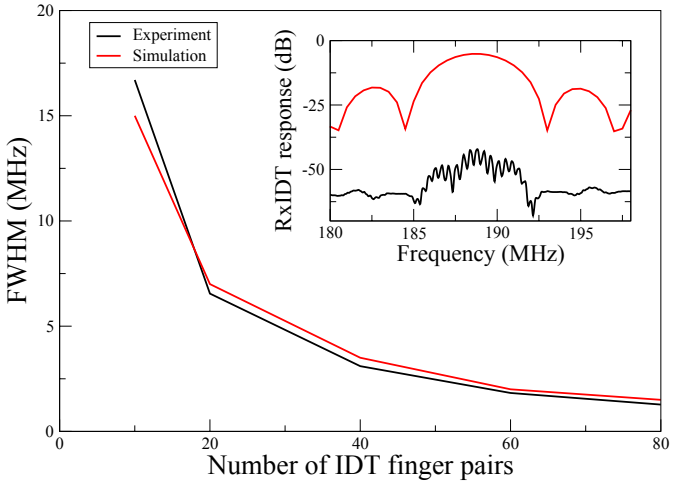

Fig. 2. Comparison of experimental and simulated FWHM of the response of transmitting and receiving IDT pairs with varying numbers of finger pairs. (Inset) Experimental and simulated frequency response for IDTs with 40 finger-pairs.

free charge is very fast, and therefore adiabatic compared to the SAW propagation. The electron density within this layer is then given as:

$$\rho_{\mathrm{e}} = \rho_{\mathrm{dop.}} + \rho_{\mathrm{SAW}} \tag{6}$$

where $\rho_{\mathrm{dop.}}$ is the charge density from the ionised dopant atoms and ρ_{SAW} is the charge density induced from the SAW, as in [4]. The bottom inset of figure 3 shows the resulting modulation in carrier concentration for a small section of a 5 μm-high ridge, showing that the SAW electric field completely depletes some regions of free charge. A self-consistent one-dimensional scattering rate model[5] was used to determine the gain characteristics of the QCL active region from Ref. [6] for a range of free-carrier concentrations, the results of which are shown in figure 3.

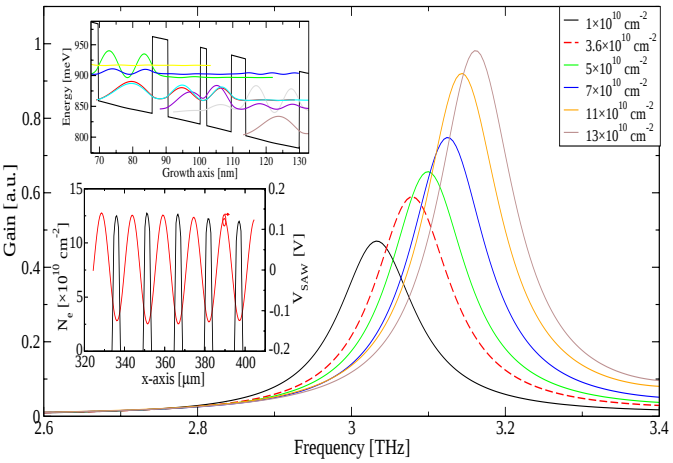

Fig. 3. Variation in the gain of the three-well resonant phonon QCL active region from [6] (top inset) for a range of free-carrier concentrations. Bottom insert: Modulation of free carrier concentration from a SAW propagating through a 5 μm high QCL ridge.

It can be seen from the main graph of Fig. 3 that changes in the carrier density within the active region, of the scale that can be produced by SAWs, are sufficient to modulate the peak gain of the QCL by $\pm$20% around the central non-modulated value, and by even more when considering a particular terahertz frequency, e.g consider the change in gain at 3.15 THz. This is quite sufficient to strongly modulate the output of the QCL in order to transmit digital data or to use in applications with coherent detection to improve signal-to-noise ratios.

V. Summary

In summary, we have presented a method for determining the strength of the modulation of free-carrier concentration within a QCL active region when a SAW is passed through the QCL ridge. The results show that the SAW contains enough energy to fully deplete areas of the QCL active region of carriers, indicating that SAW modulation of QCLs is feasible. The presented method may be exploited further to gain a better insight into the device dimensions required (e.g. QCL ridge height) to give good levels of modulation and may therefore be used as a design tool. Furthermore, the results from this model, translated into the gain and the refractive index modulation, may be used in the coupled wave description of the distributed feedback laser, in order to determine the lasing threshold conditions and the magnitude of frequency modulation achievable.

Acknowledgments

The authors would like to acknowledge funding from EPSRC (U.K.) and the European Research Council grants ‘NOTES’ and ‘TOSCA’ and valuable discussions with D. Indjin.

References

[1] W. Withayachumnankul, G. M. Png, X. X. Yin, S. Atakaramians, I. Jones, H. Y. Lin, B. S. Y. Ung, J. Balakrishnan, B. W. H. Ng, B. Ferguson, S. P. Mickan, B. M. Fisher and D. Abbot. T-ray sensing and imaging. *Proceedings of the IEEE*, 95(8):1528–1558, 2007

[2] J. F. Nye and R. B. Lindsay. *Physical Properties of Crystals: Their Representation by Tensors and Matrices*. Clarendon Press, Oxford, 1957.

[3] J.D. Cooper, A. Valavanis, Z. Ikonic, P. Harrison, and J. E. Cunningham. Stable perfectly-matched-layer boundary conditions for finite-difference time-domain simulation of acoustic waves in piezoelectric crystals. *Journal of Computational Physics*, Pending Publication.

[4] Robert L Miller. *Acoustic Charge Transport: Device Technology and Applications*. Artech House, 1992.

[5] D. Indjin, P. Harrison, R. W. Kelsall and Z. Ikonić. Self-consistent scattering theory of transport and output characteristics of quantum cascade lasers. *Journal of Applied Physics*, 91(11):9019–9026, 2002.

[6] H. Luo, S.R. Laframboise, Z.R. Wasilewski, G.C. Aers, H.C. Liu, and J.C. Cao. Terahertz quantum-cascade lasers based on a three-well active module. *Applied Physics Letters*, 90(4):041112–041112–3, 2007.